



UvA-DARE (Digital Academic Repository)

Separation of Time Scales in a Quantum Newton's Cradle

van den Berg, R.; Wouters, B.; Eliëns, S.; De Nardis, J.; Konik, R.M.; Caux, J.S.

DOI

[10.1103/PhysRevLett.116.225302](https://doi.org/10.1103/PhysRevLett.116.225302)

Publication date

2016

Document Version

Final published version

Published in

Physical Review Letters

[Link to publication](#)

Citation for published version (APA):

van den Berg, R., Wouters, B., Eliëns, S., De Nardis, J., Konik, R. M., & Caux, J. S. (2016). Separation of Time Scales in a Quantum Newton's Cradle. *Physical Review Letters*, 116(22), [225302]. <https://doi.org/10.1103/PhysRevLett.116.225302>

General rights

It is not permitted to download or to forward/distribute the text or part of it without the consent of the author(s) and/or copyright holder(s), other than for strictly personal, individual use, unless the work is under an open content license (like Creative Commons).

Disclaimer/Complaints regulations

If you believe that digital publication of certain material infringes any of your rights or (privacy) interests, please let the Library know, stating your reasons. In case of a legitimate complaint, the Library will make the material inaccessible and/or remove it from the website. Please Ask the Library: <https://uba.uva.nl/en/contact>, or a letter to: Library of the University of Amsterdam, Secretariat, Singel 425, 1012 WP Amsterdam, The Netherlands. You will be contacted as soon as possible.

Separation of Time Scales in a Quantum Newton's Cradle

R. van den Berg,¹ B. Wouters,¹ S. Eliëns,¹ J. De Nardis,¹ R. M. Konik,² and J.-S. Caux^{1,*}

¹*Institute for Theoretical Physics, University of Amsterdam, Science Park 904, 1098 XH Amsterdam, The Netherlands*

²*CMPMS Department, Brookhaven National Laboratory, Building 734, Upton, New York 11973, USA*

(Received 3 September 2015; revised manuscript received 11 March 2016; published 1 June 2016)

We provide detailed modeling of the Bragg pulse used in quantum Newton's-cradle-like settings or in Bragg spectroscopy experiments for strongly repulsive bosons in one dimension. We reconstruct the postpulse time evolution and study the time-dependent local density profile and momentum distribution by a combination of exact techniques. We further provide a variety of results for finite interaction strengths using a time-dependent Hartree-Fock analysis and bosonization-refermionization techniques. Our results display a clear separation of time scales between rapid and trap-insensitive relaxation immediately after the pulse, followed by slow in-trap periodic behavior.

DOI: 10.1103/PhysRevLett.116.225302

The study of many-body quantum physics has recently been transformed by progress achieved in experiments on ultracold atoms [1]. The context of one-dimensional (1D) bosonic gases provides a particularly fertile ground for investigating physics beyond traditional paradigms [2], with concepts such as Luttinger liquids and integrability [3] playing a primary role.

One of the main probes of cold gases is Bragg spectroscopy [4–6], which consists in applying a pulsed monochromatic laser grating onto the gas, thereby creating excitations at (multiples of) the recoil momentum q . In [7,8], a two-pulse sequence was optimized to populate the first $\pm q$ momentum satellites of a Bose-Einstein condensate. The theoretical description of this sequence relied on a two-state model where many-body dynamics were not included. In 1D, however, many-body effects are inescapable. One of the fundamental models in this context is the Lieb-Liniger (LL) gas [9] of δ -interacting bosons. This model is relevant to the description of experiments [10], most prominently the quantum Newton's cradle experiment [11], in which a Bragg pulse is used to initiate oscillations. Bragg spectroscopy has also recently been used to investigate correlated 1D Bose gases of rubidium [12] and cesium [13], where heating resulting from the Bragg pulse was measured and matched using linear response in the Lieb-Liniger gas [14].

Our main objective is to model the effects of Bragg pulses for strongly correlated 1D Bose gases, from first principles, without approximation (i.e., beyond linear response), for experimentally relevant setups. We study instantaneous pulses of varying amplitude A and wave vector q via their effect on physical observables: the time-dependent local density of the gas and the experimentally more accessible momentum distribution function (MDF). We will first focus on the Tonks-Girardeau (TG) limit [15–17] of hard-core bosons both on a periodic interval and in a harmonic trap [18–26], and then, significantly, study finite interaction effects.

Modeling Bragg pulses.—We model a Bragg pulse as a one-body potential $V(x) = V_0 \cos(qx)$ coupling to the density $\hat{\rho}(x) = \hat{\Psi}^\dagger(x)\hat{\Psi}(x)$, where the Bose fields obey the canonical equal-time commutation relations, $[\hat{\Psi}(x), \hat{\Psi}^\dagger(y)] = \delta(x-y)$. For a general Bragg pulse the gas is perturbed for a finite duration T_0 . We will, however, consider the regime where the motion of the particles during the pulse can be neglected (the Raman-Nath limit), also known as a Kapitza-Dirac pulse [27,28]. Taking the limit $T_0 \rightarrow 0$ while keeping $A = V_0 T_0$ finite, the Bragg pulse operator \hat{U}_B is given by

$$\hat{U}_B(q, A) = \exp\left(-iA \int dx \cos(qx) \hat{\Psi}^\dagger(x) \hat{\Psi}(x)\right), \quad (1)$$

where we have set $\hbar = 1$. The action of the instantaneous pulse on a ground state $|\psi_{\text{GS}}\rangle$ generates the initial state of a quantum quench [29–31]. Typical experimental pulses [11–13,32] correspond to Bragg momentum $q \sim 2\pi n$ and $A \sim 1$, where n is the mean density.

The postpulse time evolution is driven by the LL model of interacting bosons

$$H_{\text{LL}} = - \sum_{i=1}^N \frac{1}{2m} \frac{\partial^2}{\partial x_i^2} + 2c \sum_{1 \leq i < j \leq N} \delta(x_i - x_j), \quad (2)$$

either on a ring with periodic boundary conditions or in a harmonic trap with $V_{\text{trap}}(x) = \frac{1}{2} m \omega^2 x^2$. Throughout the Letter, all data is produced with $m = 1$.

Hard-core limit.—We start by considering the hard-core limit. In this limit the bosonic many-body wave function can be related through the Fermi-Bose (FB) mapping [16] to the many-body wave function of free fermions $\psi_B(\mathbf{x}; t) = \prod_{1 \leq i < j \leq N} \text{sgn}(x_i - x_j) \psi_F(\mathbf{x}; t)$, where $\mathbf{x} = \{x_j\}_{j=1}^N$ and $\psi_F(\mathbf{x}; t)$ is the usual Slater determinant of the free single-particle (SP) wave functions, $\psi_F(\mathbf{x}; t) = \det_N[\psi_j(x_i; t)] / \sqrt{N!}$. Following [19,24,26], the bosonic

one-body density matrix and thus the MDF can be computed efficiently in terms of a single determinant involving the time-dependent fermionic SP states.

In the hard-core limit we will consider two geometries: a ring geometry with no external potential and an infinite line in the presence of a parabolic trap. For the former, our ground state consists of SP plane waves, on which the Bragg pulse imprints a cosine phase due to the one-body potential,

$$\psi_j(x; t=0) = \frac{1}{\sqrt{L}} e^{-iA \cos(qx)} e^{-i\lambda_j^{\text{GS}} x}, \quad (3)$$

with ground-state rapidities $\{\lambda_j^{\text{GS}} = (2\pi/L)[-(N+1)/2 + j]\}_{j=1}^N$ forming a Fermi sea with Fermi momentum $\lambda_F = \pi n$. Note that the Bragg momentum is quantized due to the periodic boundary conditions: $q = (2\pi/L)n_q$ with $n_q \in \mathbb{N}$. Expanding Eq. (3) in plane waves, the time-dependent SP wave functions after the Bragg pulse yield

$$\psi_j(x; t) = \sum_{\beta=-\infty}^{\infty} \frac{I_{\beta}(-iA)}{\sqrt{L}} e^{-i(\lambda_j + \beta q)x} e^{-i(\lambda_j + \beta q)^2 t/2m}, \quad (4)$$

with $I_{\beta}(z)$ the modified Bessel function of the first kind.

The generalized Gibbs ensemble (GGE) [30,33] and the quench action (QA) approach [34,35] enable the study of the Bragg pulsed system (on a ring) in the thermodynamic limit ($N \rightarrow \infty$ with N/L fixed). The GGE can be constructed using the infinite number of conserved charges $\{\hat{Q}_{\alpha}\}_{\alpha=1}^{\infty}$ provided by the integrability of the LL model, with $\hat{Q}_2 = 2m\hat{H}$ and eigenvalues $Q_{\alpha}(\lambda) = \sum_{j=1}^N \lambda_j^{\alpha}$ associated to a Bethe state $|\lambda\rangle = |\lambda_1, \dots, \lambda_N\rangle$. The expectation values of the charges on the initial postpulse state can be computed using the matrix elements for the Bragg pulse between two Bethe states $|\lambda\rangle$ and $|\mu\rangle$ [36], given by

$$\frac{\langle \mu | \hat{U}_B(q, A) | \lambda \rangle}{L^N} = \det_N [I_{[(\lambda_j - \mu_k)/q]}(-iA) \delta_{\lambda_j, \mu_k}^{(q)}], \quad (5)$$

where we defined $\delta_{\lambda, \mu}^{(q)} = \delta_{(\lambda - \mu) \bmod q, 0}$. The GGE logic [30,33] then requires the expectation values of all charges to be reproduced by the equilibrated postpulse system, described by a density of rapidities $\rho_{q,A}^{\text{sp}}(\lambda)$, i.e.,

$$\lim_{\text{th}} \frac{1}{L} \langle \psi_{q,A} | \hat{Q}_{\alpha} | \psi_{q,A} \rangle = \int_{-\infty}^{\infty} d\lambda \rho_{q,A}^{\text{sp}}(\lambda) \lambda^{\alpha}, \quad (6)$$

for all $\alpha \in \mathbb{N}$. This leads to the stationary-state distribution [37,38]

$$\rho_{q,A}^{\text{sp}}(\lambda) = \frac{1}{2\pi} \sum_{\beta \in \mathbb{Z}} [\theta(\lambda - \beta q + \lambda_F) - \theta(\lambda - \beta q - \lambda_F)] |I_{\beta}(iA)|^2, \quad (7)$$

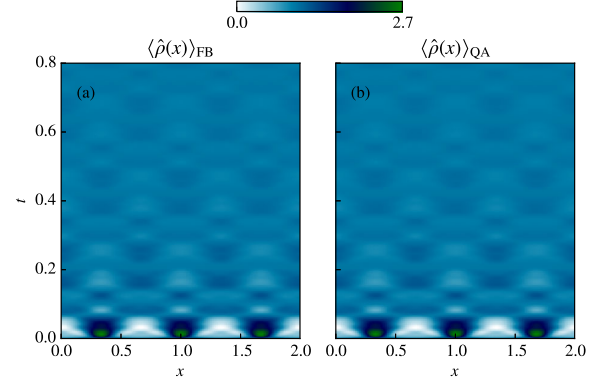


FIG. 1. Time evolution of the density after a Bragg pulse with $q = 3\pi$ and $A = 1.5$, computed by (a) the FB mapping and (b) the QA approach. The relative differences between the two results due to finite-size effects are less than 0.4%.

where θ is the Heaviside step function. The saddle-point distribution is a sum of copies of the ground-state density of rapidities, $\rho_{\text{GS}}(\lambda) = (1/2\pi)[\theta(\lambda + \lambda_F) - \theta(\lambda - \lambda_F)]$, shifted by multiples of q and weighted by the modified Bessel functions. This form of the stationary state is consistent with the QA approach [39], which furthermore provides access to the time evolution of local observables by summing over particle-hole excitations in the vicinity of $\rho_{q,A}^{\text{sp}}(\lambda)$ [34,35,40].

The time-dependent density of the hard-core gas in the thermodynamic limit can be obtained via the QA approach or with the FB mapping. Interestingly, one can obtain the identical result from the noninteracting limit of the Tomonaga-Luttinger model with a quadratic band-curvature term. The nonlinear Luttinger liquid theory (NLL) [41,42] result for finite interactions reads [43]

$$\langle \hat{\rho}(x, t) \rangle = n + \sqrt{K} \sum_{\beta \neq 0} J_{\beta} \left(-2\sqrt{K}A \sin \frac{\beta q^2 t}{2m^*} \right) \times \cos(\beta q x) \frac{\sin(\beta q v_s t)}{\pi \beta q t / m^*}, \quad (8)$$

with $J_{\beta}(z)$ the Bessel function of the first kind. Here, K is the Luttinger parameter, v_s the sound velocity, and m^* the renormalized effective mass. Surprisingly, the noninteracting limit with $K = 1$, $v_s = \lambda_F/m$, and $m^* = m$, reproduces the exact TG result. The validity of Eq. (8) for finite interactions is discussed in the last section of this Letter. We compare the TG result against finite-size FB computations for $N = 50$ in Fig. 1 and observe relative differences of the order of 0.4% due to finite-size effects. In the Raman-Nath limit, the postpulse density at $t = 0$ is unaltered from the flat ground-state profile. A sharp density profile then develops, mimicking the one-body cosine potential, followed by relaxation back to a flat profile at time scales $t \sim m/q\lambda_F = (qv_s)^{-1}$.

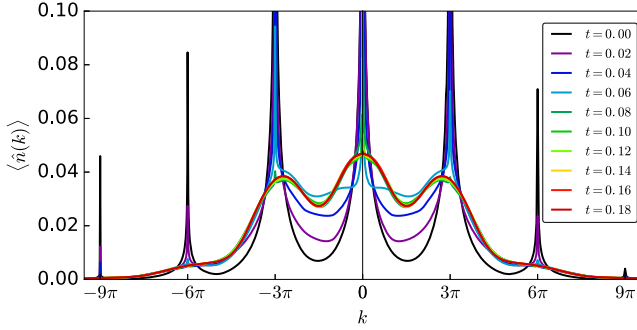


FIG. 2. Time evolution of the MDF after a Bragg pulse with $q = 3\pi$ and $A = 1.4$, computed with the QA approach (left) and the FB mapping (right). Because the FB mapping treats a finite system ($N = 50$) the momenta are quantized, causing less-pronounced peaks for short times. All other results are in excellent agreement with the QA computations.

The QA approach also provides access to the time evolution of the MDF [46,47]. The result is plotted in Fig. 2 along with the FB result for $N = 50$. Except for minor disagreements in the sharp peaks due to finite-size effects, the large-system-size dynamics after the Bragg pulse is again well captured by a $N = 50$ FB mapping. At $t = 0$, one can show that the MDF (for any value of c) is simply a sum of copies of the ground-state MDF [48], with a small- k divergence $\langle \hat{n}(k) \rangle_{\text{GS}} \sim k^{-1/2}$ in the TG limit, centered around multiples of q . Similar to the initial MDF, the late-time distribution behaves like a superposition of independent peaks shifted to multiples of q , yielding a characteristic ghostlike shape [11]. The width of each satellite shows no dependence on the value of q , and is only influenced by the choice of A [49]. Since in the limit of $A \rightarrow 0$ the MDF reduces to the ground-state time-independent distribution, the broadening can be ascribed to interactions between particles belonging to different satellites.

Next, we will use the FB mapping to investigate how these observations translate to the more experimentally relevant geometry of a harmonic trapping potential, with the Hamiltonian $H_{\text{trap}} = H_{\text{LL}} + \sum_{i=1}^N \frac{1}{2} m \omega^2 x_i^2$ and ω the trapping frequency. The ground-state SP harmonic oscillator wave functions are given by

$$\psi_j(x) = \frac{1}{\sqrt{2^j j!}} \left(\frac{m\omega}{\pi} \right)^{1/4} e^{-m\omega x^2/2} H_j(\sqrt{m\omega}x), \quad (9)$$

for $j = 0, \dots, N-1$, with $H_j(x)$ denoting the Hermite polynomials. Using the propagator for the quantum harmonic oscillator [50], we compute the time evolution of the SP wave functions [51],

$$\begin{aligned} \psi_j(x; t) &= \sum_{\beta=-\infty}^{\infty} I_{\beta}(-iA) e^{-i\beta q \cos(\omega t)[x + (\beta q/2m\omega) \sin(\omega t)]} \\ &\times \psi_j \left[x + \frac{\beta q}{m\omega} \sin(\omega t) \right] e^{-i\omega(j+1/2)t}. \end{aligned} \quad (10)$$

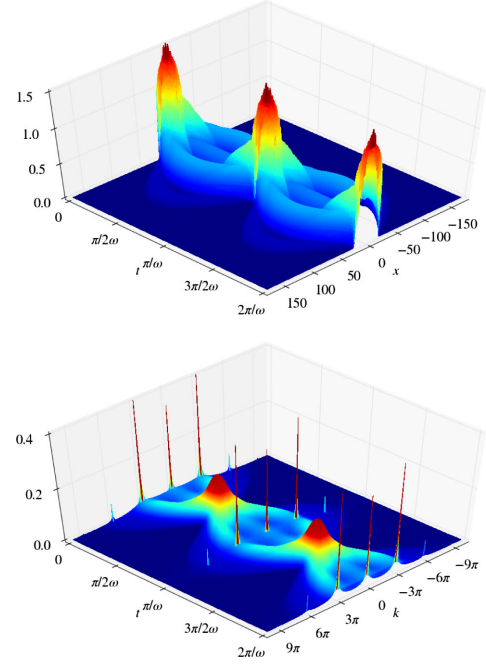


FIG. 3. The time evolution of the density (top) and MDF (bottom) in the trap, computed with the FB mapping for $N = 50$, $\omega = 10/N$, $A = 1.5$, and $q = 3\pi$.

The SP wave functions are periodic in time with period $2\pi/\omega$, which is reflected in observables such as the density and the MDF. This periodicity is expected to be broken by finite- c interactions and anharmonicities in the trapping potential. The time evolution of the density and the MDF during one period is shown in Fig. 3, where the contributions from particles belonging to different satellites are clearly distinguishable. During the initial stages of relaxation (and around multiples of $t = \pi/\omega$) the density shows strong oscillations and the initially sharply peaked MDF relaxes rapidly to a broadened shape. This pre-relaxation is well separated from the trap-induced collective periodic motion, suggesting that it is governed by the same physics as relaxation on a ring.

In Fig. 4 the density at early stages in the oscillation cycle is compared to that on a ring, the latter being supplemented by a local density approximation (LDA) to account for the classical expansion of the gas in the trap [52,53]. The initial density profile is accurately reproduced by the LDA, except for small differences near the edges originating from gradients in the local density not accounted for within the LDA [54–57]. Note, however, that these differences do not stay confined to the edges and propagate towards the center as time progresses.

The short-time MDF in the trap and ring geometry is shown in Fig. 5 up to $t = 0.015\pi/\omega$. The initial distributions are nearly identical, after which the MDFs dephase in a similar fashion to a (pre)relaxed ghostlike shape. The strong similarities can be attributed to the short-range correlations characterizing the postquench steady state.

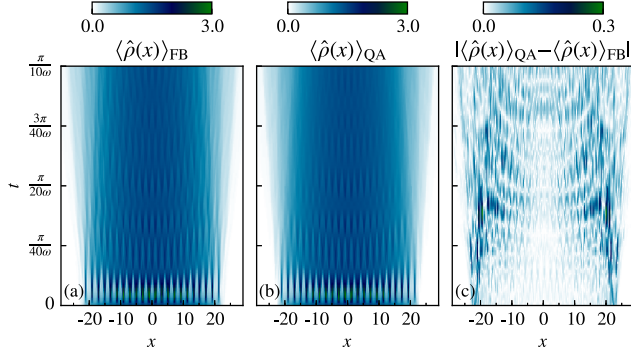


FIG. 4. Time evolution of the density in a trap, computed with (a) the FB mapping for $N = 50$ particles and (b) the QA approach on a ring with a LDA accounting for the trap. The difference between the two results is shown in (c). The Bragg pulse parameters are set to $A = 1.5$ and $q = \pi$ with $\omega = 10/N$.

Large-distance effects due to the trap geometry lead to discrepancies only at low momenta. The time scale associated to this (pre)relaxation is estimated to be the time it takes for a boson traveling with the speed of sound to traverse one density oscillation induced by the Bragg pulse, $t \sim 2\pi/qv_s$. Considering conditions similar to the Newton's cradle experiment, we estimate the short time scale to be of the order of $10 \mu\text{s}$. This estimate is of the same order of magnitude as the pulse duration used in [11], suggesting that interaction effects can be important for longer pulses. This will be treated in future publications.

Finite interactions.—We now extend our results to finite interactions by considering the dual fermionic model to Eq. (2) [58–60],

$$H_F = - \sum_{i=1}^N \frac{1}{2m} \frac{\partial^2}{\partial x_i^2} - \frac{1}{m^2 c} \sum_{1 \leq i < j \leq N} \delta''(x_i - x_j). \quad (11)$$

Using a self-consistent time-dependent Hartree-Fock (TDHF) approximation [62,63], we have performed finite- c calculations of the density and MDF, shown in Figs. 6(a), 6(c), and 6(d). The equilibrium Hartree-Fock computation yields an effective mass of the plane-wave quasiparticles given by $m^* = m/(1 - 2n/mc)$ [62,63], suggesting that the out-of-equilibrium finite- c results can be rescaled according to $t \rightarrow t(1 - 2n/mc)$, to produce the same time-dependent behavior as in the $c \rightarrow \infty$ limit. This is confirmed by the rescaled results shown in Fig. 6(b). Furthermore, the density at $x = 0$ shows an enhancement of the high-density regions for decreasing c , consistent with a model for attractive fermions. The NLL result of Eq. (8) reproduces the correct time scaling for large values of c , but is unable to account for the increased density oscillations. This discrepancy can be attributed to the neglected irrelevant operators which cannot be justified by a renormalization group argument in out-of-equilibrium settings. In Fig. 6(c) the relaxation of the MDF at $k = 0, q, 2q$ shows a delay in relaxation

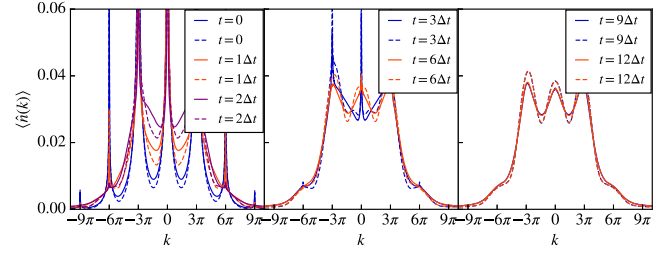


FIG. 5. Time evolution of the MDF for the trap geometry (solid lines) and the ring geometry (dashed lines), obtained with the FB mapping for $N = 50$ particles. The trapping frequency is set to $\omega = 10/N$, and we used $A = 1.5$ and $q = 3\pi$. The time step Δt is set to $\pi/800\omega$.

consistent with a reduced sound velocity $v_s = \pi n/m (1 - 2n/mc + \dots)$. Finally, the relaxed MDF in Fig. 6(d) depicts increasingly condensed satellites for smaller c , as is expected from bosons with decreasing repulsive interactions.

Conclusion.—We have developed a theoretical description of the Bragg pulse for one-dimensional Bose gases and shown that the time evolution of physical observables for a Bragg pulsed Lieb-Liniger gas in a trap is characterized by two well-separated time scales. The shortest time scale is dominated by the trap-insensitive contact interactions and causes a substantial broadening of the momentum distribution well before the collective motion due to the presence of the trap sets in. Our work can be extended to include finite interaction effects in harmonic traps [64], and it opens

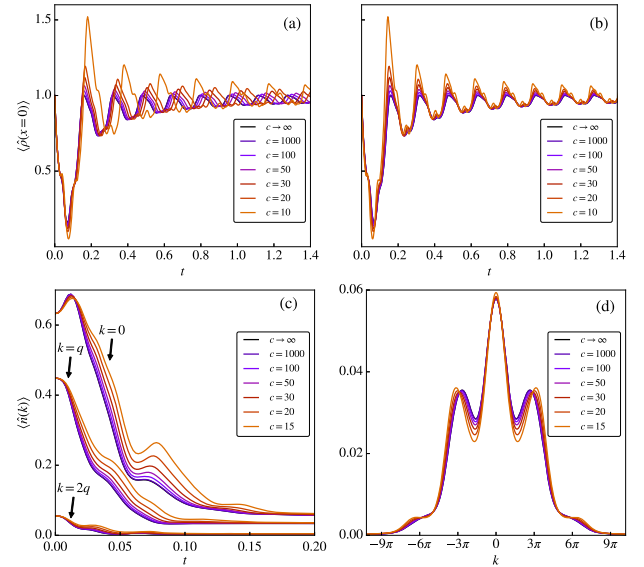


FIG. 6. Finite- c results using TDHF for the ring geometry. (a), (b) Time evolution of the density at $x = 0$ for $N = 50$, $A = 1$, and $q = 2\pi$. In (b) the results of (a) are rescaled according to $t \rightarrow t(1 - 2n/mc)$. (c) Time evolution of the MDF at $k = 0, q, 2q$ for $N = 50$, $A = 1.3$, and $q = 3\pi$ and (d) the relaxed MDF at $t = 0.4$.

up the possibility to study the influence of interactions on more general pulse protocols and to incorporate finite-temperature effects.

We thank M. Brockmann, E. A. Demler, N. J. van Druten, V. Gritsev, F. Meinert, H.-C. Nägerl, J. Schmiedmayer, F. E. Schreck, D. Weiss, and J. van Wezel for useful discussions. This work was supported by the Netherlands Organisation for Scientific Research (NWO) and the Foundation for Fundamental Research on Matter (FOM), and forms part of the activities of the Delta-Institute for Theoretical Physics (D-ITP). The contribution to this work by R. M. K. was supported by the U.S. Department of Energy, Office of Science, Basic Energy Sciences, Materials Sciences and Engineering Division. R. v. d. B. also acknowledges support for visiting the CMPMS Division at Brookhaven National Lab, a facility supported by the U.S. Department of Energy, Office of Basic Energy Sciences. We are grateful for support from the Centre de Recherches Mathématiques of the Université de Montréal.

*J.S.Caux@uva.nl

- [1] I. Bloch, J. Dalibard, and W. Zwerger, *Rev. Mod. Phys.* **80**, 885 (2008).
- [2] M. A. Cazalilla, R. Citro, T. Giamarchi, E. Orignac, and M. Rigol, *Rev. Mod. Phys.* **83**, 1405 (2011).
- [3] T. Giamarchi, *Quantum Physics in One Dimension* (Oxford University Press, New York, 2004).
- [4] P. J. Martin, B. G. Oldaker, A. H. Miklich, and D. E. Pritchard, *Phys. Rev. Lett.* **60**, 515 (1988).
- [5] J. Stenger, S. Inouye, A. P. Chikkatur, D. M. Stamper-Kurn, D. E. Pritchard, and W. Ketterle, *Phys. Rev. Lett.* **82**, 4569 (1999).
- [6] R. Ozeri, N. Katz, J. Steinhauer, and N. Davidson, *Rev. Mod. Phys.* **77**, 187 (2005).
- [7] Y.-J. Wang, D. Z. Anderson, V. M. Bright, E. A. Cornell, Q. Diot, T. Kishimoto, M. Prentiss, R. A. Saravanan, S. R. Segal, and S. Wu, *Phys. Rev. Lett.* **94**, 090405 (2005).
- [8] S. Wu, Y.-J. Wang, Q. Diot, and M. Prentiss, *Phys. Rev. A* **71**, 043602 (2005).
- [9] E. H. Lieb and W. Liniger, *Phys. Rev.* **130**, 1605 (1963).
- [10] M. Olshanii, *Phys. Rev. Lett.* **81**, 938 (1998).
- [11] T. Kinoshita, T. Wenger, and D. S. Weiss, *Nature (London)* **440**, 900 (2006).
- [12] N. Fabbri, M. Panfil, D. Clément, L. Fallani, M. Inguscio, C. Fort, and J.-S. Caux, *Phys. Rev. A* **91**, 043617 (2015).
- [13] F. Meinert, M. Panfil, M. J. Mark, K. Lauber, J.-S. Caux, and H.-C. Nägerl, *Phys. Rev. Lett.* **115**, 085301 (2015).
- [14] M. Panfil and J.-S. Caux, *Phys. Rev. A* **89**, 033605 (2014).
- [15] L. Tonks, *Phys. Rev.* **50**, 955 (1936).
- [16] M. Girardeau, *J. Math. Phys. (N.Y.)* **1**, 516 (1960).
- [17] E. Haller, M. Gustavsson, M. J. Mark, J. G. Danzl, R. Hart, G. Pupillo, and H.-C. Nägerl, *Science* **325**, 1224 (2009).
- [18] A. Minguzzi and D. M. Gangardt, *Phys. Rev. Lett.* **94**, 240404 (2005).
- [19] R. Pezer and H. Buljan, *Phys. Rev. Lett.* **98**, 240403 (2007).
- [20] D. M. Gangardt and M. Pustilnik, *Phys. Rev. A* **77**, 041604 (2008).
- [21] D. Muth, B. Schmidt, and M. Fleischhauer, *New J. Phys.* **12**, 083065 (2010).
- [22] C. Schenke, A. Minguzzi, and F. W. J. Hekking, *Phys. Rev. A* **84**, 053636 (2011).
- [23] G. E. Astrakharchik and L. P. Pitaevskii, *Europhys. Lett.* **102**, 30004 (2013).
- [24] M. Collura, S. Sotiriadis, and P. Calabrese, *Phys. Rev. Lett.* **110**, 245301 (2013).
- [25] E. Quinn and M. Haque, *Phys. Rev. A* **90**, 053609 (2014).
- [26] F. Cartarius, E. Kawasaki, and A. Minguzzi, *Phys. Rev. A* **92**, 063605 (2015).
- [27] P. L. Kapitza and P. A. M. Dirac, *Proc. Cambridge Philos. Soc.* **29**, 297 (1933).
- [28] D. L. Freimund, K. Aflatooni, and H. Batelaan, *Nature (London)* **413**, 142 (2001).
- [29] P. Calabrese and J. Cardy, *Phys. Rev. Lett.* **96**, 136801 (2006).
- [30] M. Rigol, V. Dunjko, V. Yurovsky, and M. Olshanii, *Phys. Rev. Lett.* **98**, 050405 (2007).
- [31] A. Polkovnikov, K. Sengupta, A. Silva, and M. Vengalattore, *Rev. Mod. Phys.* **83**, 863 (2011).
- [32] R. E. Sapiro, R. Zhang, and G. Raithel, *Phys. Rev. A* **79**, 043630 (2009).
- [33] M. Rigol, V. Dunjko, and M. Olshanii, *Nature (London)* **452**, 854 (2008).
- [34] J.-S. Caux and F. H. L. Essler, *Phys. Rev. Lett.* **110**, 257203 (2013).
- [35] J. De Nardis, B. Wouters, M. Brockmann, and J.-S. Caux, *Phys. Rev. A* **89**, 033601 (2014).
- [36] See Supplemental Material at <http://link.aps.org/supplemental/10.1103/PhysRevLett.116.225302>, Sec. A, for a derivation of the matrix elements and initial state on the ring.
- [37] G. Bevilacqua, V. Biancalana, Y. Dancheva, T. Mansour, and L. Moi, *J. Math. Phys. (N.Y.)* **52**, 033508 (2011).
- [38] See Supplemental Material at <http://link.aps.org/supplemental/10.1103/PhysRevLett.116.225302>, Sec. B, for a derivation of the stationary-state distribution from a generalized Gibbs ensemble.
- [39] See Supplemental Material at <http://link.aps.org/supplemental/10.1103/PhysRevLett.116.225302>, Sec. B, for a derivation of the stationary-state distribution from the Quench Action approach.
- [40] J. De Nardis, L. Piroli, and J.-S. Caux, *J. Phys. A* **48**, 43FT01 (2015).
- [41] A. Imambekov and L. I. Glazman, *Science* **323**, 228 (2009).
- [42] A. Imambekov, T. L. Schmidt, and L. I. Glazman, *Rev. Mod. Phys.* **84**, 1253 (2012).
- [43] See Supplemental Material at <http://link.aps.org/supplemental/10.1103/PhysRevLett.116.225302>, Sec. C, which includes Refs [44,45], for the derivation of the nonlinear Luttinger Liquid result for the time evolution of the density.
- [44] A. V. Rozhkov, *Phys. Rev. B* **77**, 125109 (2008).
- [45] G. N. Watson, *A Treatise on the Theory of Bessel Functions*, 2nd ed. (Cambridge University Press, Cambridge, England, 1944) (republished by Cambridge University Press, Cambridge, England, 1995).
- [46] J. De Nardis and J.-S. Caux, *J. Stat. Mech.* (2014) P12012.

- [47] See Supplemental Material at <http://link.aps.org/supplemental/10.1103/PhysRevLett.116.225302>, Sec. D, for the time evolution of the momentum distribution function on a ring derived using the Quench Action approach.
- [48] See Supplemental Material at <http://link.aps.org/supplemental/10.1103/PhysRevLett.116.225302>, Sec. E, for the derivation of the momentum distribution at $t = 0$ for arbitrary interactions.
- [49] See Supplemental Material at <http://link.aps.org/supplemental/10.1103/PhysRevLett.116.225302>, Sec. F, for the equilibrated momentum distribution on a ring for different values of q and A .
- [50] F. G. Mehler, *J. Reine Angew. Math.* **1866**, 161 (1866).
- [51] See Supplemental Material at <http://link.aps.org/supplemental/10.1103/PhysRevLett.116.225302>, Sec. G, for the derivation of the time-evolved single-particle states in the trap.
- [52] A. S. Campbell, D. M. Gangardt, and K. V. Kheruntsyan, *Phys. Rev. Lett.* **114**, 125302 (2015).
- [53] See Supplemental Material at <http://link.aps.org/supplemental/10.1103/PhysRevLett.116.225302>, Sec. H, for details of the local density approximation.
- [54] K. V. Kheruntsyan, D. M. Gangardt, P. D. Drummond, and G. V. Shlyapnikov, *Phys. Rev. A* **71**, 053615 (2005).
- [55] A. H. van Amerongen, J. J. P. van Es, P. Wicke, K. V. Kheruntsyan, and N. J. van Druten, *Phys. Rev. Lett.* **100**, 090402 (2008).
- [56] J. Armijo, T. Jacqmin, K. Kheruntsyan, and I. Bouchoule, *Phys. Rev. A* **83**, 021605 (2011).
- [57] T. Jacqmin, J. Armijo, T. Berrada, K. V. Kheruntsyan, and I. Bouchoule, *Phys. Rev. Lett.* **106**, 230405 (2011).
- [58] T. Cheon and T. Shigehara, *Phys. Rev. Lett.* **82**, 2536 (1999).
- [59] D. Sen, *Int. J. Mod. Phys. A* **14**, 1789 (1999).
- [60] This form of the interaction potential is technically only correct for variational calculations such as Hartree-Fock approximations. For a more general form of the interaction potential valid for all orders of $1/c$ see [61].
- [61] See Supplemental Material at <http://link.aps.org/supplemental/10.1103/PhysRevLett.116.225302>, Sec. I, for details of the time-dependent Hartree-Fock approximation.
- [62] J. Brand and A. Y. Cherny, *Phys. Rev. A* **72**, 033619 (2005).
- [63] A. Y. Cherny and J. Brand, *Phys. Rev. A* **73**, 023612 (2006).
- [64] M. Gattobigio, *J. Phys. B* **39**, S191 (2006).